Journal of Visualization, Vol. 9, No. 3 (2006)257-264

Visualization and PIV Measurement of the Flow around and inside of a Falling Droplet

Ninomiya, N.*[1] and Yasuda, K.*[2]

*1 Department of Energy and Environmental Science, Graduate School of Engineering, Utsunomiya University, 7-1-2 Yoto, Utsunomiya, Tochigi 321-8585, Japan. E-mail: nino@utmu.jp
*2 ASMO Co. Ltd., 90 Umeda, Kosai, Shizuoka 431-0493, Japan.

Received 28 October 2005
Revised 24 January 2006

Abstract : Although the phenomena related to the multiphase flow can be found in many kinds of industrial and engineering applications, the physical mechanism of the multiphase flow has not been investigated in detail. The major reason for the lack of data in the multiphase flow lies in the difficulties in measuring the flow quantities of the multiple phases simultaneously. Presently, the visualization and the PIV measurement have been carried out about the both phases of the liquid-liquid two-phase flow. The difference in the refractive indices makes the visualization in the vicinity of the boundary of the multiple phases very difficult. In this study, the refractive index of the aqueous phase has been equalized to that of the oil phase by adjusting the concentration of the aqueous solution. As for the surrounding fluid, silicon oil is chosen and as for the droplet, the aqueous solution of glycerol is prepared whose refractive index matches that of silicon oil. Both phases are seeded with neutrally buoyant particles. The droplet is slightly colored with Rhodamine B so that the position of the invisible droplet can be identified. The difference in the background brightness in both phases helps PIV algorithm in distinguishing the motions in each phases. The results show the details of the flow structures both around and inside of a falling droplet simultaneously.

Keywords : Visualization, PIV, Index matching, Droplet, Two-phase flow.

1. Introduction

Multiphase flow has been one of the most difficult and, at the same time, one of the most practically important phenomena in the fluid mechanics. Many studies for the multiphase flow have been conducted in order to investigate the details about the momentum and material transfer at the interface. Numerical studies, such as Dandy and Leal (1989), have revealed many kinds of flow characteristics about two- phase flow. Even though the measurements about the surrounding fluid, such as Cieslinski et al. (2005), have been extensively carried out, only a few results have been reported about the flow near the boundary and the flow inside of a bubble or a droplet. This is mainly because the discontinuity of the refraction index at the phase interface makes the measurement or even the visualization very difficult.

Recent developments in the visualization technique and the improvements in the imaging devices make the great progress in the measurement techniques. Especially, those by the particle image velocimetry (PIV) and by the particle tracking velocimetry (PTV) are outstanding. Nevertheless, the PIV or PTV measurements in the multiphase flow are still limited to the

examination of continuous phases. The reason of the lack of data for the dispersed phases is because the visualization itself is still very difficult with the refraction at the interface of the multiphase flow. Yamauchi et al. (2000) have succeeded in measuring the flow field inside of the water droplet falling through the stationary oil by compensating the complex distortion caused by the refraction at the boundary of a droplet assuming that the droplet is spherical or ellipsoidal. Presently, the authors of this study have carried out the PIV measurements of the flow around and inside of the falling droplet simultaneously under various flow conditions by using the index matching technique, as was used by Knapp and Bertrand (2005). By adjusting the refractive index of the water to that of the oil, the refraction at the interface is completely eliminated. Furthermore, the droplet is slightly colored by the fluorescent dye and thus the shape of the droplet is re-visualized. As a result, the visualization and the PIV measurements of the two-phase flow around and inside of a falling droplet have been carried out and the detailed flow characteristics are investigated.

2. Measurement Procedure

In order to visualize the flow around and inside of a droplet simultaneously, the refractive indices of the inner and outer phases should be matched. As the refractive index of silicon oil is 1.3999, whereas that of water is 1.3330, the refractive index of water phase can be matched by introducing some miscible substance of higher refractive index. In this study, the glycerol, whose refractive index is 1.4716 and is also immiscible to silicon oil, is chosen for the refractive index matching substance. Figure 1 shows the change of the refractive indices of silicon oil and glycerol solution of various concentrations. It is obvious that the glycerol solution of higher concentration takes higher refractive index. The refractive index of ordinary liquid gets smaller with higher temperature, but its gradient is different with liquid. Thus the refractive index of glycerol solution of adequate concentration and temperature can be matched with that of the silicon oil. Presently, 50 % glycerol solution is chosen so that its refractive index matches that of the silicon oil, i.e., 1.3999, at room temperature of 20 deg.

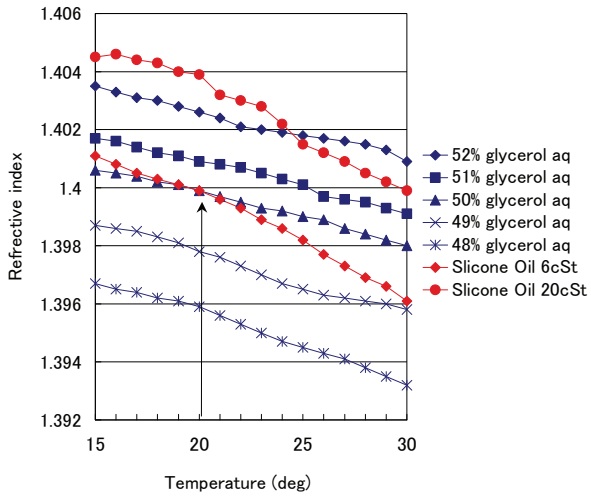

Fig. 1. Refractive indices of fluids.

The physical properties of the working fluids used in this study are summarized in Table 1. As for the oil phase, silicon oil of 6 cSt is chosen so that the difference in viscosity of the fluid does not affect the measurement condition drastically. As shown in Table 1, the refractive indices of 50 % aqueous solution of glycerol and silicon oil of 6 cSt are exactly matched. For the tracer particle in each phase, nylon 6 and polyethylene are selected whose specific densities are exactly the same as those of fluids. Thus, the motions of each fluid can be visualized perfectly. In order to examine

various flow conditions, silicon oil of 20 cSt is also examined. Even though the refractive index and the specific density of silicon oil of 20 cSt are slightly bigger than those of silicon oil of 6cSt, their values are quite close and any apparent difference could not be found during the experiment and thus no special correction is made for the measurement with silicon oil of 20 cSt.

Table 1. Physical properties of fluids at 20 deg.

	50 % Glycerol aq.	Silicon Oil 6cSt	Silicon Oil 20cSt
Refractive index	1.3999	1.3999	1.4030
Viscosity	6.70 m Pa s	5.40 m Pa s	18.2 m Pa s
Specific density	1.130	0.925	0.950
Tracer particle	Nylon 6 ρ = 1.13, 20 μm	Polyethylene ρ = 0.925, 15 μm	Polyethylene ρ = 0.925, 15 μm

Figure 2 shows the schematic view of experimental apparatus. Silicon oil of 6 cSt is filled in the reservoir of 100 x 100 x 500 mm, inside of which a thin cylindrical wall of Plexiglas is placed in order to avoid the effect of corner of the container. To illuminate the tracer particles, double-pulsed Nd-YAG laser is used and the beam is expanded by the cylindrical lens and then focused into thin sheet by the sheet forming optics as shown in Fig. 2. The typical image obtained in this study is shown in Fig. 3. As the refractive indices of both phases are perfectly matched, the boundary of the droplet is no more visible. Thus, in this study, the droplet is slightly colored by Rhodamine B so that the shape of the droplet can be distinguished by the fluorescence. The image of the droplet is captured by CCD camera that has the resolution of 1K x 1K and then directly transferred to PC.

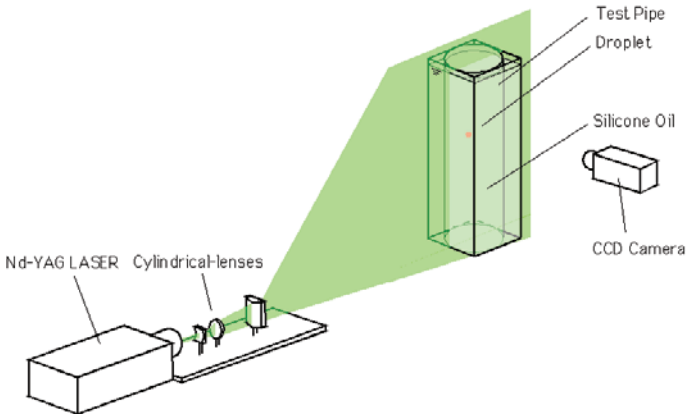

Fig. 2. Experimental apparatus.

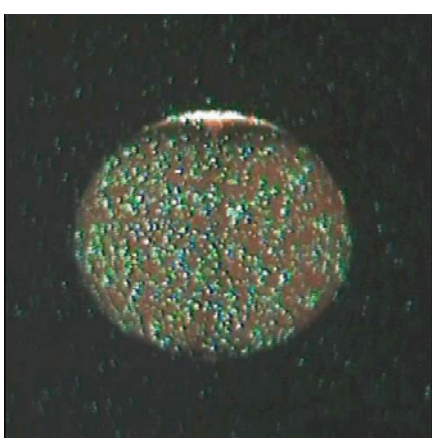

Fig. 3. Typical image of a droplet.

Before calculating the velocity field around and inside of a falling droplet, the size and the position of the droplet are determined from the images shown in Fig. 3. As the droplet is slightly colored by the fluorescent dye, the droplet can be identified as slightly bright region. In order to eliminate the images of the tracer particles, the smoothing is applied to the original image. Then the derivative of brightness is taken in order to enhance the outline of the droplet. Finally, by fitting the ellipse to the outline by the least square method, the center and the radii in major and minor axes of the droplet are obtained. The terminal velocity is calculated from the displacement and the time interval and then the non-dimensional parameters, such as the aspect ratio of the droplet, drag coefficient C_D, Reynolds number Re, Morton number Mo and Eötvös number Eo or Bond number Bo. According to the Grace's diagram, excerpted from Clift et al. (1978), shown in Fig. 4, the present droplet is plotted a little bit in ellipsoidal zone and the measured aspect ratio of 0.88 agrees well with the diagram.

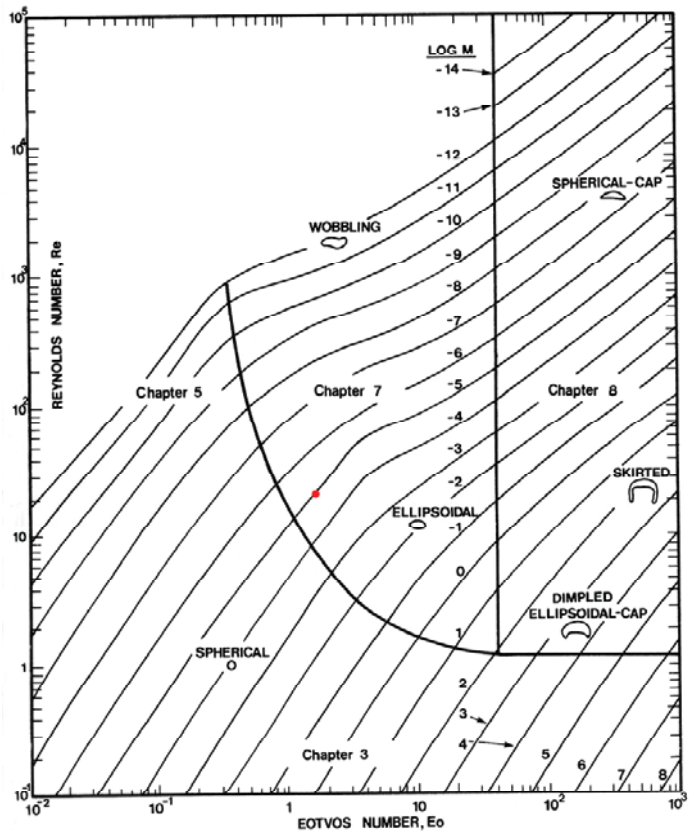

Fig. 4. Grace's diagram for the shape of bubble (● indicates the present condition).

3. PIV Results

The typical result of the PIV measurement in this study is shown in Fig. 5. According to the preliminary experiments, the terminal velocity of a droplet is almost constant and the flow patterns are almost steady while it travels. The 30 samples are averaged in obtaining the results. The two circles drawn in Fig. 5 designate the outlines of a droplet illuminated by the double-pulsed laser light sheets. The descending flows in the falling droplet and in the wake of a droplet are clearly seen. The counter-rotating vortices in the wake of a droplet are not seen with this Reynolds number of 25.1. It is obvious that the ambient fluid in front of the droplet is swept away by the droplet.

Even though the flow pattern inside of a droplet forms the counter-rotating vortices and is quite typical to this type of flow, it cannot be seen in Fig. 5. In order to show the detail of the flow

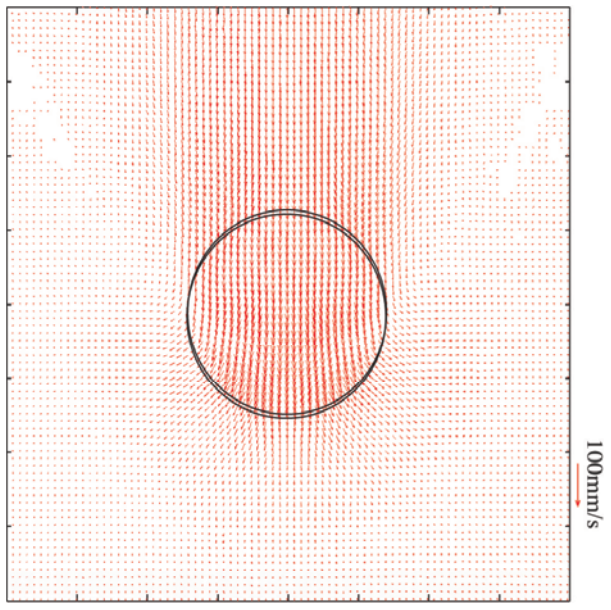

Fig. 5. PIV result (flow at a fixed coordinates).

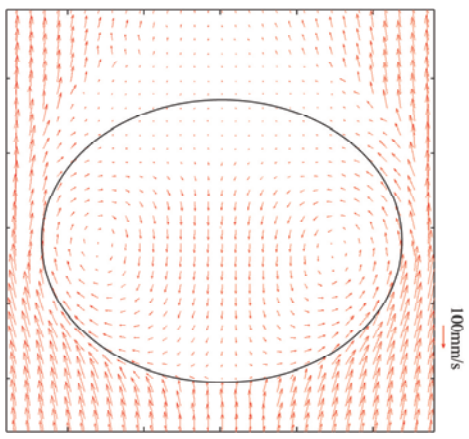

(a) $d = 8.06\ mm$
$V_\infty = 122.0\ mm/s$
$C_D = 1.34$

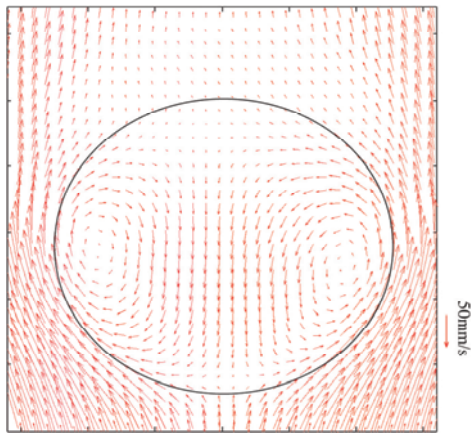

(b) $d = 6.52\ mm$
$V_\infty = 88.3\ mm/s$
$C_D = 2.07$

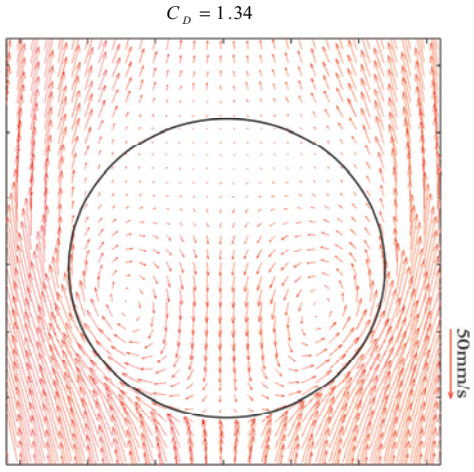

(c) $d = 3.99\ mm$
$V_\infty = 53.1\ mm/s$
$C_D = 3.502$

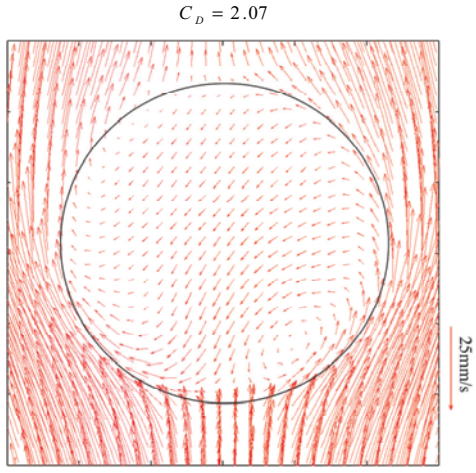

(d) $d = 2.35\ mm$
$V_\infty = 12.3\ mm/s$
$C_D = 38.456$

Fig. 6. PIV results (flow relative to a droplet).

patterns inside a droplet, the terminal velocity of a droplet is subtracted from the PIV result. Thus, the flows relative to a droplet are obtained and shown in Figs. 6. These are the results for the different sizes of a droplet. Figure 5 corresponds to Fig. 6(b) of the diameter d = 6.52 mm in major axis. The counter-rotating vortices inside of a droplet are now clearly seen and the fluid in front of a droplet flows along the droplet. The stagnant region behind a droplet is also very clear in Figs. 6.

As the size of a droplet gets smaller from Fig. 6(a) to Fig. 6(d), the terminal velocity gets smaller, the drag coefficient C_D gets bigger, and the shape of a droplet gets more spherical. It is said that, as the size of a droplet gets smaller, the surface tension by the contaminant accumulated at the downstream side of a droplet affects the flow pattern inside of a droplet and the center of the counter-rotating vortices move toward the upstream side of a droplet. This phenomenon is quite obvious in Figs. 6, but the flow pattern for the smallest droplet in Fig. 6(d) is somewhat asymmetric. This asymmetry may be caused by the buoyancy effect by the heat of laser.

In order to emphasize the shift of the position of the counter-rotating vortices, the vorticity distributions are calculated from the PIV results. The typical results are shown in Figs. 7. It is seen that the maximum of the vorticity does not coincide with the vortex core but is located in the vicinity of the boundary of the droplet, where the shear rate is expected to be relatively high. Even though the maximum of the vorticity does not exactly match with the center of the vortex, the vorticity takes relatively high value around the vortex core region. It is clearly seen from Figs. 7 that the position of the vortex shifts toward the upstream side for the smaller droplet.

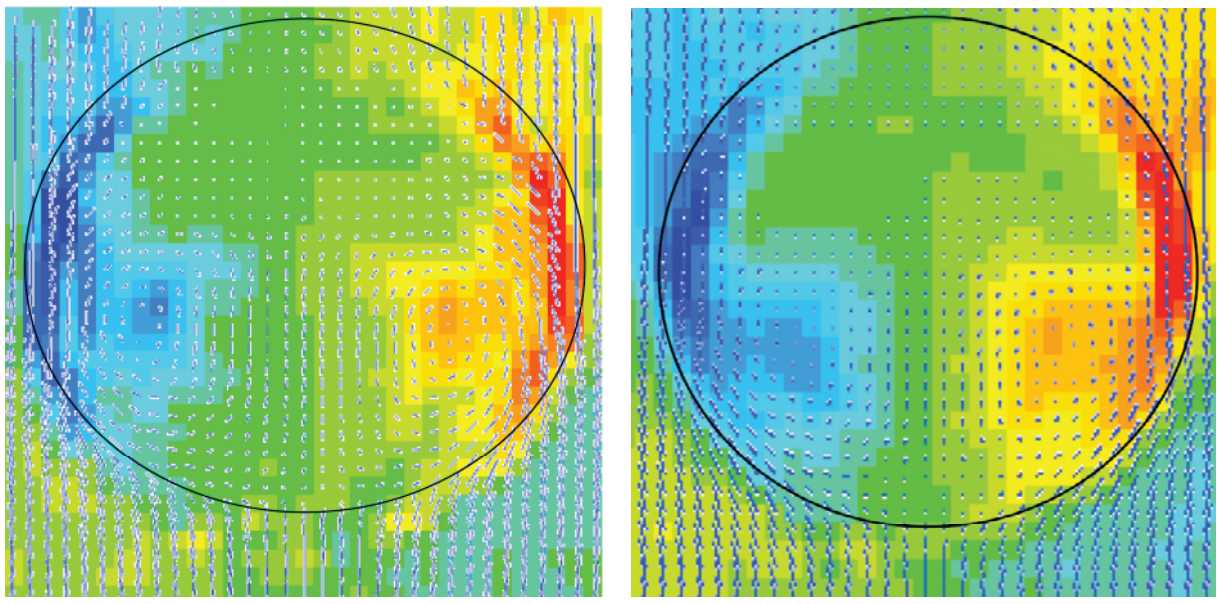

(a) $d = 8.06\ mm$, $V_\infty = 122.0\ mm/s$, $C_D = 1.34$

(b) $d = 3.99\ mm$, $V_\infty = 53.1\ mm/s$, $C_D = 3.502$

Fig. 7. Vorticity distributions around and inside of a droplet.

4. Flow Patterns inside of a Droplet

In previous studies about the droplet or the bubble, the flow field around the droplet or the bubble has been extensively examined. Presently, the authors of this study have succeeded in visualizing the flow field around and inside of a droplet simultaneously. Thus, the details of the flow patterns inside of a falling droplet are examined in this section.

Figure 8 is the typical photograph of the flow visualization done in this study. In this study, the droplet has been formed by dropping the adequate amount of the aqueous solution of glycerol by a

pipette placed at the top of the reservoir. In preparing the aqueous solution in a pipette, the upper half portion is colored by Rhodamine B and the bottom half portion is colored by Fluoresein in order to obtain this photograph. As the diffusion between differently colored solutions is much smaller than the convection in a droplet, thus the layers with different color are folded while it travels. Consequently, the flow pattern inside of a droplet can be visualized very clearly.

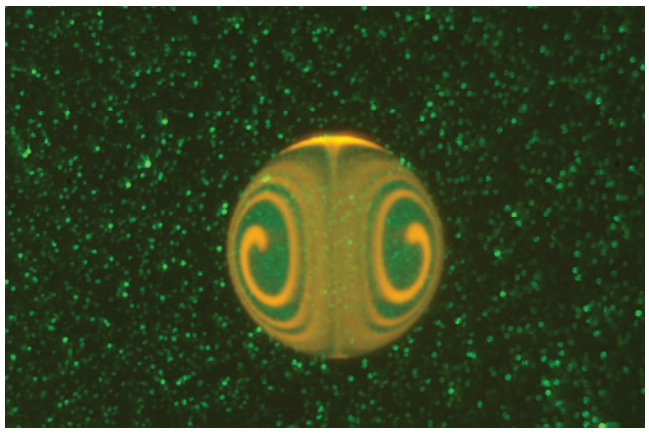

Fig. 8. Typical flow pattern inside of a droplet.

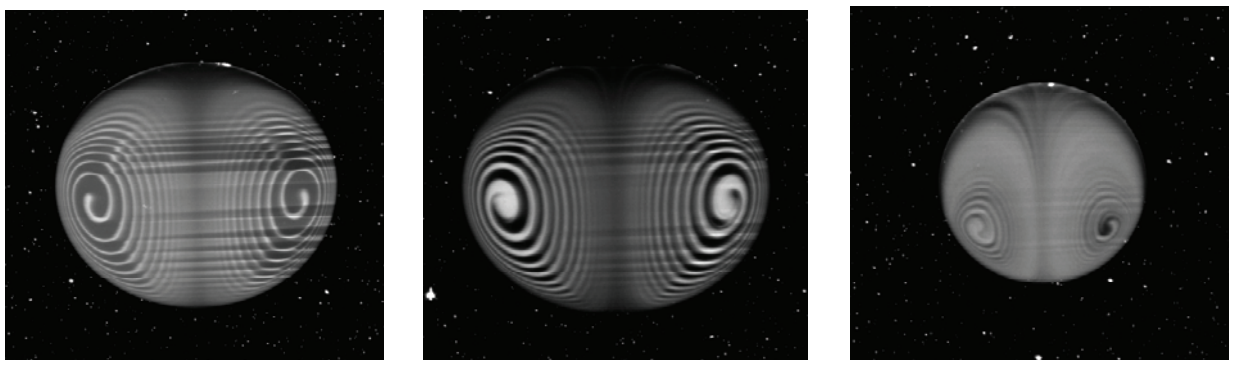

Fig. 9. Flow patterns inside of a droplet.

The flow visualization results for the different sizes of a falling droplet are shown in Figs. 9. The flow patterns inside of a falling droplet are clearly seen as the streak of the colored aqueous solution. It can be seen that as the size of a droplet is bigger, the terminal velocity becomes faster and thus the drag coefficient becomes smaller. When the size of a droplet is small, the surface tension by the contaminant, which has been accumulated at the downstream side of a droplet, prevents the convection along the boundary of the droplet and thus the counter-rotating flow in the droplet cannot involve the downstream stagnant region. As a result, the centers of the counter-rotating vortices are located somewhat forward. This feature is very clear in the smaller diameter case in Fig. 9(c) and is almost indistinguishable in the bigger droplet in Fig. 9(a).

5. Conclusion

In order to investigate the details of the flow around and inside of a falling droplet simultaneously, the refractive index of the water phase is perfectly matched to that of the oil phase and thus the refraction at the boundary of a water droplet falling in oil is completely avoided. By introducing the

tracer particles, which are neutrally buoyant to each phase, and by slightly coloring the droplet by the fluorescent dye, the flow around and inside of a falling droplet and the position of a droplet are clearly visualized. As a result of the PIV measurement using this visualization technique, the details of the flow around and inside of a falling droplet are obtained simultaneously.

Thus, the followings are the conclusions of this study:

1) The index matching technique is very effective in visualizing the inner phase of the liquid-liquid two-phase flow.

2) As for the PIV measurement, the difference in the background brightness of the slightly colored drop and the non-colored surrounding fluid helps in distinguishing the flows in each phase.

3) The typical flow patterns, such as the counter-rotating vortices inside of a droplet, the flow pushed away by the droplet in front of a droplet and the stagnant region behind a droplet, are clearly visualized by the PIV results.

4) The visualization of the flow pattern inside of a droplet reveals the fact that the flow inside of a smaller droplet is more strongly affected by the surface tension by the contaminant accumulated at the downstream end of a droplet and thus the centers of the counter-rotating vortices inside of a droplet shift toward the upstream side.

References

Dandy, D. S. and Leal, L. G., Buoyancy-driven Motion of a Deformable Drop through a Quiescent Liquid at Intermediate Reynolds Numbers, Journal of Fluid Mechanics, 208 (1989), 161-192.

Cieslinski, J. T., Polewski, J. and Szymczyk, J. A., Flow Field around Growing and Rising Vapour Bubble by PIV Measurement, Journal of Visualization, 8-3 (2005), 209-216.

Yamauchi, M., Uemura, T. and Ozawa, M., Velocity Distributions Inside and Outside of A Water Drop in Oil, Application of Laser Techniques to Fluid Mechanics, CD-ROM, (2000), 1-6.

Knapp, Y. and Bertrand, E., Particle Imaging Velocimetry Measurements in a Heart Simulator, Journal of Visualization, 8-3 (2005), 217-224.

Clift, R., Grace, J. R. and Weber, M. E., Bubbles, Drops and Particles, (1978), Academic Press.

Author Profile

Nao Ninomiya: He received his M.Sc. (Eng) in Mechanical Engineering in 1988 from University of Tokyo. He also received his Ph.D. in Mechanical Engineering in 1992 from University of Tokyo. He worked as a JSPS researcher since 1989. He worked as a research associate in Department of Mechanical Systems Engineering, Utsunomiya University since 1991 and has been an associate professor in Department of Energy and Environmental Science, Graduate school of Engineering, Utsunomiya University since 1996. His research interests are Quantitative Visualization including PTV, PIV, LIF, Spark Tracing Method and Advanced Heat Transfer and Fluid Flow.

Kazuma Yasuda: He received his Bachelor (Eng.) from Department of Mechanical Systems Engineering, Faculty of Engineering, Utsunomiya University in 2004 and received his M.Sc. (Eng.) degree from Department of Energy and Environmental Science, Graduate School of Engineering, Utsunomiya University in 2006. He now works at ASMO Co. Ltd.